PPEDCRF: Privacy-Preserving Enhanced Dynamic CRF for Location-Privacy Protection for Sequence Videos with Minimal Detection Degradation

Bo Ma, Jinsong Wu *(Senior Member, IEEE)*, Weiqi Yan, Catherine Shi, Minh Nguyen

***Abstract*—Dashcam videos collected by autonomous or assisted-driving systems are increasingly shared for safety auditing and model improvement. Even when explicit GPS metadata are removed, an attacker can still infer the recording location by matching background visual cues (e.g., buildings and road layouts) against large-scale street-view imagery. This paper studies location-privacy leakage under a background-based retrieval attacker, and proposes PPEDCRF, a privacy-preserving enhanced dynamic conditional random field framework that injects calibrated perturbations only into inferred location-sensitive background regions while preserving foreground detection utility.**

PPEDCRF consists of three components: (i) a dynamic CRF that enforces temporal consistency to discover and track location-sensitive regions across frames, (ii) a normalized control penalty (NCP) that allocates perturbation strength according to a hierarchical sensitivity model, and (iii) a utility-preserving noise injection module that minimizes interference to object detection and segmentation. Experiments on public driving datasets demonstrate that PPEDCRF significantly reduces location-retrieval attack success (e.g., Top-k retrieval accuracy) while maintaining competitive detection performance (e.g., mAP and segmentation metrics) compared with common baselines such as global noise, white-noise masking, and feature-based anonymization. The source code is in https://github.com/mabo1215/PPEDCRF.git.

***Index Terms*—Object Detection, Dynamic Conditional Random Field, Privacy-preserving, Automotive Vision Systems**

I. Introduction

Dashcam videos from autonomous and advanced driver-assistance systems (ADAS) are routinely uploaded for safety investigation, incident auditing, and data-driven model improvement. Removing explicit metadata such as GPS coordinates is necessary but not sufficient for privacy protection: the background of a single frame may contain distinctive visual landmarks that can be matched to large-scale street-view databases. Fig. 1 illustrates a representative threat, where a dashcam frame can be linked to a geographically-tagged street-view image, thereby revealing the recording location.

This work focuses on *location privacy* in driving videos under a realistic background-based matching attacker. Unlike identity privacy (e.g., face anonymization), location privacy leakage can be triggered by non-human background cues (buildings, road signs, skyline, and layout), and naive defenses such as global masking or heavy blurring often damage downstream perception tasks. We aim to reduce location leakage while preserving the utility of object detection and segmentation models used in ADAS pipelines.

Bo Ma is with Auckland University of Technology, New Zealand, Email address: rcn4743@aut.ac.nz.

Jinsong Wu is with the Department of Electrical Engineering, Universidad de Chile, Chile.

Weiqi Yan, Catherin Shi and Minh Nguyenare with Auckland University of Technology, New Zealand.

A. Threat Model

We consider an adversary who obtains a dashcam frame (or a short clip) with GPS and other metadata removed, but the background content remains visible. The adversary has access to a large street-view database in which each image is associated with a geo-tag (latitude/longitude). The adversary extracts background visual features from the query frame and performs image retrieval (or feature matching) against the street-view database to infer the most likely recording location.

Formally, let q denote a query dashcam frame and $\mathcal{D} = \{(s_i, \ell_i)\}_{i=1}^{N}$ denote a street-view database with images s_i and location labels ℓ_i. The attacker computes an embedding $f(\cdot)$ and returns a ranked list by similarity $\mathrm{sim}(f(q), f(s_i))$. An attack succeeds if the ground-truth location of q is within the top-k retrieved results (Top-k accuracy / Recall@k). Our defense aims to reduce the attacker's retrieval success while preserving detection/segmentation performance for ADAS.

B. Research Range

There have been several research works connected to privacy-related applications with object detection and tracking, including face recognition [1], [2], autonomous driving, and robot navigation [3], and location detection [4]. Previous object detection and tracking approaches were based on machine vision. A real-time video can include multiple objects. It is difficult and challenging to protect the privacy of sensitive targets such as pedestrians when detecting targets. In addition, we cannot simply remove those objects from the images since they will be required for their applications. Thus, the aim of the research is to preserve the privacy of object locations in images while maintaining object recognition and tracking.

C. Related Work

In the real-time dynamic position detection task, the characteristics of the deep network constitute different degrees of obstacles to the detection task [5]. At the same time, due to camera or network delay, the data source video may be spliced in time and space, and this error also constitutes an obstacle to the object detection task. Obstacles to deep network

Fig. 1: Images taken by a dashcam can be matched with an image from Google Street View.

features will cause the ability of certain specific neural network architectures to be unable to process a large number of feature sets from streaming video sets in real time.

In general object detection tasks, two-stage detectors have been achieved with the advancement of region-based CNN (RCNN) [6] and Faster RCNN [6]. For privacy-preserving in Faster RCNN, Ren [7] proposed an anonymization method with Faster RCNN that modifies the raw video to remove privacy or sensitive part in the target frames in a video stream. After that, Liu [8] proposed a new method based on Faster RCNN, his work also removed sensitive information to protect the sensitive information in medical images, but it will also impact inference data retraining.

In order to overcome this defect, Zhou proposed [9] the privacy protection method that utilized MTCNN [10] model to locate the sensitive position and revise affinities with noise resistance rather than remove the sensitive information. In addition, Wang mentioned [11] that videos with low-resolution and in fast movement scenarios are still challenging because the backbone network in Convolutional Neural Network (CNN) can drop to a deficient performance under low-resolution scenarios, and the current Convolutional Neural Network can not map and fit the image data-set with deficient quality and almost identical pixel information.

A few existing works have discussed optimizing the loss function and increasing entropy while reducing the leakage of sensitive data [12]. A loss function is accommodated to evaluate how effective the specific algorithm works for the given data [13]. If the predictions deviate beyond the ground, loss or cost values will increase. However, through randomization, if differential privacy is employed, there are still limitations through using the existing mechanisms (e.g., Laplace or exponential mechanisms) in the broader differential-privacy literature to detect visual objects [14]. In this case, quantifying and searching the bounding boxes of an object is an unknown task. In addition, quantifying and locating the partitioned parts to be identified from the background in the video is undetermined. Partitioning undetermined backgrounds is one of the limitations in detecting privacy-preserving sensitive objects, which is also the research motivation of this paper.

D. Motivations and Contributions

This paper makes the following contributions:

- We formulate location-privacy leakage in dashcam videos as a background-based retrieval attack and evaluate privacy risk using Top-k retrieval metrics under realistic street-view matching.
- We propose PPEDCRF, a dynamic CRF-based framework that discovers and propagates location-sensitive regions across frames via temporal consistency, enabling region-level privacy protection instead of global masking.
- We introduce a Normalized Control Penalty (NCP) mechanism to allocate perturbation strength based on a hierarchical sensitivity model, providing an explicit control knob to trade off privacy protection and perception utility.
- Extensive experiments show that PPEDCRF reduces location-retrieval attack success while maintaining competitive object detection and segmentation performance compared with several privacy baselines.

1) Whether δ provides the minimum amount of data required to obtain (ε, δ)-differential privacy in object detection.
2) what would occur for the detection task if $\varepsilon \geq 1$.

As mentioned above, Gaussian distribution-based privacy preservation approaches are a number of limitations, especially if $\varepsilon \to 0$, using Gaussian perturbation to achieve $(0, \delta)$-differential privacy obviously exceeds the capabilities of the classic scheme. In the theorem of differential privacy, the standard deviation $\sigma = \Theta(\frac{1}{\sqrt{\varepsilon}})$ increases if $\varepsilon \to \infty$, there will be $\sigma = \frac{\Delta}{2\delta}$ in $(0, \delta)$-differential privacy. The condition [15] with $\varepsilon \to 0$ is used to analyze (ε, δ)-differential privacy.

In privacy-oriented object detection, it is necessary to determine the classes of sensitive objects and regions of the digital images before adding noises. For example, adding overdose white noises, and salt or pepper noises will protect the privacy parts but destroy the image, which cannot be utilized for visual object detection and tracking. We will discuss the issues and unfold our contributions from three aspects:

1) We prove that in the dynamic object detection task δ in ε, δ-differential privacy is sub-optimal, and it can achieve a higher privacy environment, i.e., especially on the condition with $\varepsilon \to 0$. The aim of this step is to explore the relationship between changing the differential privacy parameters and the probability of privacy leakage.
2) We show that the standard deviation of the Gaussian

perturbation that provides (ε, δ)-differential privacy can be scaled as $\Omega(\frac{1}{\sqrt{\varepsilon}})$, which can be used to establish classification matrix. We establish a classification matrix by scaling the standard deviation of the Gaussian perturbation to establish classification management for the relationship between privacy protection classes and regions so that the association between privacy features and non-sensitive features is clearer.

3) We use Dynamic Conditional Random Fields(DCRF) to establish the association of privacy objects between different frames in the sequence images, and at the same time preserve the privacy objects themselves.
4) We analyze the privacy leakage and use the Gaussian mechanism to sample the privacy objects and provide a parameter penalty named Normalized Control Penalty(NCP) mechanism to control the private feature information in the inference results, so as to reduce the occurrence of privacy leakage.

This means that the scaling $\Theta(\frac{1}{\sqrt{\varepsilon}})$ is provided by the classical Gaussian mechanism within the range $\varepsilon \in (0, 1)$ cannot exceed any bounded interval. Based on this assumption, have been classified according to their entropy, and we then generate the noises following their probability distribution. noise injected into feature representation for release and training.

II. Our Proposed Methods

A. Overview Architecture

To protect the sensitive area while ensuring that the object detection framework keeps detection accuracy, the deep learning model's training and inference work can still run stably, and we try to find a solution in the classification stage to break through the existing problems and limitations. Based on the ideas from works [16][17], our work is inspired by connecting the given labels of sensitive objects with spatial dependencies, and at the same time using this kind of existing class associations to determine the goal of inference. Finally, the image data are mapped, and the corresponding sensitive areas are processed separately.

According to the above thoughts, we propose the solution named Privacy-preserving Enhanced Dynamic Conditional Random Field (PPEDCRF) method including five parts as shown in Figure 2.

1) In the first step, we collect the sensitive data, since the training set and data classifications depend on the data characteristics, such as street signboards, landmark buildings, and so on. Then, we use MOT [18] or others as the test set for our experiments.
2) In the second step, we train the labeled sensitive data with the categories of objects input to an enhanced dynamic conditional random field in order to prepare for the discernibility matrix (DM) to find similar areas in the test image and link the classes of the sensitive data together. The DM contains the adjacent information, which will assist PPEDCRF to retrain and adjust weights or other parameters in future steps.
3) In the third step, we need to collect the test data and send it to the PPEDCRF. In the final stage, our experiment selected samples from three public data sets [19].
4) In the fourth step, we use the discernibility matrix and classes to restructure the DM corresponding to the given test images. Then, we import them into the existing object detection model, such as Faster R-CNN [6], YOLO [20]. After the object detection, the framework will return similar regions or objects with our matched results. Thus, we add generated noises into the sensitive region inside the test images.
5) The last step is optional. In this step, we examine whether the test images can match the scene's location. For comparison, we propose a Normalized Control Penalty(NCP) to measure the loss between the ground truth result and inference result, where the NCP integrates the existing scale-invariant feature transform (SIFT) [21] and structural similarity [22] approach to test the images with the similar locations.

B. Subsampling for Privacy Noise Data

The first step is to collect privacy features from incoming data, where we assess the privacy level of the classes of sensitive objects and generate the noises when training the model. The randomization is defined as $M : \mathbb{S} \to \mathbb{G}$ with Gaussian distribution $\mathbb{S}$ and the domain $\mathbb{G}$ which satisfies (ε, δ)-differential privacy. We define the input data sets as $i \in \mathbb{S}$, and we add the noise from any subset of outputs $D \in \mathbb{R}$ with the cost $Privacy[M(r) \in \mathbb{G}] \subseteq Privacy[M(r') \in L]$.

The output perturbation of ε-differential privacy is obtained according to $\delta \subseteq \frac{\Delta l_2 log\frac{1.135}{\delta}}{\varepsilon}$.

We propose the privacy-preserving method, where the sampled subset $R_t \leq G(a, b)$ and $G(a, b)$ are in the Gaussian domain with class pair (a, b). The noise n_t is updated itself as $\Delta n_t^g = n_t^g - n_t$, where n_t^g is the noise from sampling space and n_t is the noise in time t. s is randomization quantity and m_t is random number in time t. We expand the Gaussian distribution as

$$n_{t+1} = \frac{1}{m}\{\Sigma_{g=0}^{m_t} \frac{\Delta n^g}{max(<\Psi(a), \Psi(b)>, \frac{\|\Delta n^g\|_2}{P})} + u_t\}. \quad u_t \in \mathcal{N}(0, \varepsilon^2 P^2) \tag{1}$$

$$\tilde{z}_t = z_t + M_t \odot \epsilon_t, \qquad \epsilon_t \sim \mathcal{N}(0, \sigma_t^2 I), \tag{2}$$

Here $z_t = f(I_t)$ is the extracted feature representation, M_t is the PPEDCRF-inferred sensitive mask in feature/patch space, and $\sigma_t = \sigma_0 \cdot \alpha_t$ is controlled by NCP.

By calculating the entropy from a set of input data, our method is employed to analyze the object region of interest (ROI), and there exist labels with privacy features. For object detection. The entropy [23] for input training data is obtained via calculating the kernelized distance between the image samples and the center of feature space which is measured via Renyi entropy. When the quality of entropy has been confirmed, we can measure the relationship between privacy classes and the objects it belongs to from available information. This approach includes the Renyi differential function

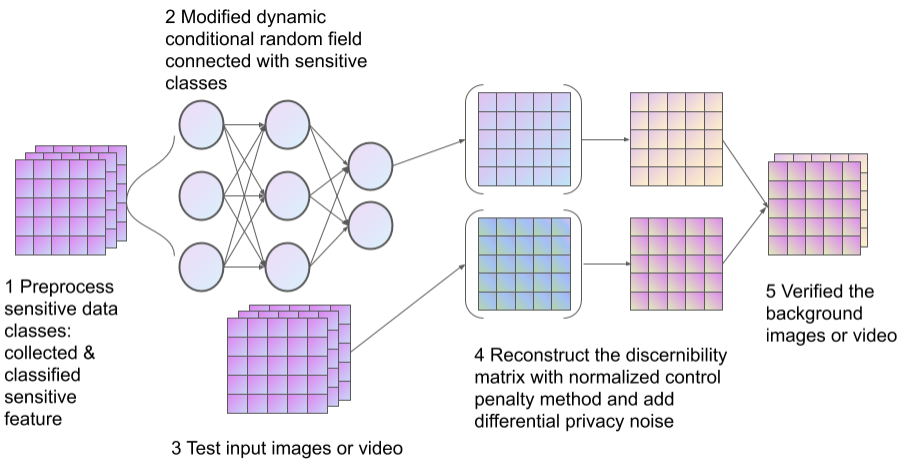

Fig. 2: The Architecture of Privacy-preserving Enhanced Dynamic Conditional Random Field(PPEDCRF) for Segmentation and Object Detection

(RDF) and the measurement of given samples. Therefore, we get the distance between the most sensitive objects and the lowest ones as the maximum of the privacy, and then we give the privacy score corresponding to the sensitive objects.

Definition 1 (Privacy Cost(Budget))**.** *From the Renyi differential function, the quality of privacy noise from (Equation 1) can be defined as* c *according to its effectiveness, let* $PB(c)$ *be the privacy cost(also named privacy budget) score which can descript the privacy noise level where* c *is instantiated from the exists tuple* (a, b)*. A* c *in privacy cost(budget) is with two relevant data-sets* a *and* b *if* c *is instantiated by* a, b*, which contains an execution tuple* (a', b')*. In order to predicate tuple* (a, b) *and the privacy cost(budget)* c*,* c *is required to have such a property that* (a, b) *contains an execution tuple* (a', b')*, which is able to predicate* c*. The privacy budget* c *is calculated as*

$$\begin{aligned} PB(c) &= p(a, b|n_t) = \prod_{t=1}^{T} p(a_t, b_t|n_t) \\ &= \prod_{t=1}^{T} p(b_t|b_{t+1}, n_t) p(a_t|b_t, n_t) \end{aligned} \tag{3}$$

Lemma 1 (Transfer function for sensitive region and privacy score)**.** *In transfer function the cumulative sum of predictive region* ω *as* $\Delta\omega_{t-1}$ *and sensitive region* $\rho_{1:T}$ *from states 1 to* T *according to their privacy score, those results can be deduced from the image data sets and hyper parameter* $P_n(\eta, \tau, G)$*.*

Equation 3 is used to compute the entropy of input data. The privacy budget score is a value of privacy noise level, and the n_t is the noise produced from Equation 1. And those classes of sensitive images and the labels of classes need to be collected, the process is $C(a, b|n_t)$. This is a measure to discover the privacy leakage from the input data. Then the data is imported into the PPEDCRF for calculating the privacy budget score. In the proposed algorithm 1, after the algorithm computes out the privacy score, according to the Theorem 1, we can get the sequence for sensitive region ρ and predictive region ω in the target image.

Lemma 2 (Masked Gaussian noise increases sensitive-feature distance)**.** *Let* $z_t \in \mathbb{R}^d$ *be the feature of a query frame and* $s \in \mathbb{R}^d$ *be a candidate street-view feature. Let* $M_t \in \{0, 1\}^d$ *be a binary mask selecting sensitive components and* $\epsilon_t \sim \mathcal{N}(0, \sigma_t^2 I)$*. Define the sanitized feature* $\tilde{z}_t = z_t + M_t \odot \epsilon_t$*. Then the expected squared distance satisfies*

$$\mathbb{E}\big[\|\tilde{z}_t - s\|_2^2\big] = \|z_t - s\|_2^2 + \sigma_t^2 \|M_t\|_0, \tag{4}$$

where $\|M_t\|_0$ *is the number of selected sensitive components.*

Proof. By expansion, $\|\tilde{z}_t - s\|_2^2 = \|z_t - s\|_2^2 + 2\langle z_t - s,\, M_t \odot \epsilon_t\rangle + \|M_t \odot \epsilon_t\|_2^2$. Since ϵ_t is zero-mean Gaussian, the cross term has zero expectation. Moreover, $\mathbb{E}\|M_t \odot \epsilon_t\|_2^2 = \sigma_t^2 \|M_t\|_0$ because only masked dimensions contribute. □

Theorem 1 (Expected similarity reduction under masked feature noise)**.** *Assume the attacker uses a linear similarity score* $\mathrm{sim}(a, b) = a^\top b$ *on features. With* $\tilde{z}_t = z_t + M_t \odot \epsilon_t$ *and* $\epsilon_t \sim \mathcal{N}(0, \sigma_t^2 I)$*, the expected similarity is preserved in mean:* $\mathbb{E}[\tilde{z}_t^\top s] = z_t^\top s$*, but its variance increases as*

$$\mathrm{Var}(\tilde{z}_t^\top s) = \sigma_t^2 \|M_t \odot s\|_2^2, \tag{5}$$

which increases ranking uncertainty for location retrieval.

Proof. $\tilde{z}_t^\top s = z_t^\top s + (M_t \odot \epsilon_t)^\top s$. The second term has zero mean, so the expectation equals $z_t^\top s$. Its variance equals $\mathrm{Var}((M_t \odot \epsilon_t)^\top s) = \sigma_t^2 \|M_t \odot s\|_2^2$ by properties of Gaussian noise. □

C. Observation and classification from sequence images with conditional random fields

In the second stage of Figure 2, the input images will be processed via a modified dynamic conditional random field, where we can create the observation stream to monitor the input sequence images, and the stream can be used in Conditional Random Field (CRF) to analyze the status of observed images. Then we will use Euclidian distance to

measure the feature distance from existing labeling images to target images to be classified.

We assume that the data a are the input street video, based on the observation data from time 0 to t, and the posterior probability of the segment s_t is modeled via using Conditional Random Field (CRF). While labeling the given segments, the labels follow the conditional Markov model [24], and the output random variables constitute a Markov random field. Conditional Random Field(CRF) can be viewed as a generalization of maximum entropy Markov models to labeling problems [25].

$$M(C_t(a)|i_{1:t}, C_t(b), a \neq b) = M(p_t(a)|i_{1:t}, C_t(b), b \in F_a), \tag{6}$$

where $i_{1:t} = i_1, i_2, \dots i_t$ are the observation data from time 1 to t. We assume that $C_t(a)$ and $C_{t+1}(a)$ are the target sequence images at time t and $t+1$ and the class categories are unknown, $C_t(b)$ is an existing classified object in certain classes.

Therefore, the method in the Hammersley-Clifford theorem [26] is used to obtain the posterior probability of the $C_t(a)$ class. After maximum likelihood estimation, the data-set follows (7) if it follows a Gibbs distribution:

$$\begin{aligned} M(C_t(a)|i_{1:t}) \propto \exp\{-\sum_{a\in A} R_x(C_t(a)|i_{1:t}) \\ + \sum_{b\in F_a} R_{a,b}(C_t(a), C_t(b))\}. \end{aligned} \tag{7}$$

The single-domain $R_a(s_t(X)|I_{1:t})$ reflects the observation of a single shot from 1 to t and $s_t(X)$ is the single-shot sequences and X is the input data-sets, while the dual-domain potential $R_{a,b}(C_t(a), p_t(b))$ is to form a continuous observation by applying the spatial constraints. It is assumed that the pairwise constraints are independent of the observed data to simplify the calculation. Spatial connectivity $S_{a,b}(C_t(a), C_t(b))$ is imposed by using the dual-domain potential,

$$R_{a,b}(C_t(a), C_t(b)) \propto S_{a,b}(C_t(a), C_t(b)) \tag{8}$$

and

$$R_{a,b}(C_t(a), C_t(b)) = \frac{1}{\|a-b\|^2}(1 - \sigma(C_t(a) - C_t(b))), \tag{9}$$

where $\|a-b\|^2$ is Euclidian distance, $\sigma(C_t(a) - C_t(b))$ is a Kronecker Delta function [27]. Thus, two neighborhoods $C_t(a), C_t(b)$ possibly belong to the same class. The spatial constraint becomes stronger with decreasing distances between the data-sets classes.

In order to express the dynamic CRF(DCRF) of the continuous segments, the state transition probability of the segmentation field is also approximated by using the distribution defined on the single-domain and dual-domain data sets.

$$\begin{aligned} M(C_{t+1}|p_t) \propto \exp\{-\sum_{a\in A} R_a(C_{t+1}(a)|C_t(G_a)) \\ + \sum_{b\in F_a} R_{a,b}(C_{t+1}(a), C_{t+1}(b))\}, \end{aligned} \tag{10}$$

where G_a specifies t_{th} in the data-set, its adjacent shots have an impact on all adjacent domains, $C_t(G_a)$ means that $C_t(b), t \in G$ holds for a group of G, $R_a(C_{t+1}(a)|C_t(G_a))$ is used to model the state transition of a single position. For a pair of data-sets $R_{a,b}(C_{t+1}(a), C_{t+1}(b))$, Eq.(10) gives its spatial constraints, F_a is the unequal set in the neighborhood G_a.

The size may be different for $X \notin F_a$, $a \in G_a$. For the convenience of discrimination, F_a is called as the spatial neighborhood, and G_a is the temporal neighborhood.

$$R_a(C_{t+1}(a)|C_t(G_a)) = \frac{1}{|F_a|}\sum_{b\in F_a} R_a(C_{t+1}(a), C_t(b)) \tag{11}$$

$$R_a(C_{t+1}(a)|C_t(G_a)) \propto S_a(C_{t+1}(a)|C_t(b)) \tag{12}$$

and

$$S_a(C_{t+1}(a)|C_t(b)) = \frac{1}{\| a-b \|^2 + \rho^2}(1 - \sigma(C_{t+1}(a) - C_t(b))), \tag{13}$$

where $|F_a|$ represents the size of the set, $R_a(C_{t+1}(a)|C_t(G_a))$ is the potential prediction results which are used to predict its nearest group from existing classes through the match with temporal constraints. The parameter ρ is the time-dependent statement of the sequence images. Generally, if the input sequence data changes slowly, the quantity of ρ will be small correspondingly, and vice versa.

From Eq.(7) to Eq.(13) we can predict whether target $p_t(\omega)$ and $C_{t+1}(\omega)$ belongs to existing classified $C_t(\rho)$. Then we can create the spatial observation as a discernibility matrix(DM).

We assume that the spatial observations are independently and identically distributed, and the observation model $q(l_t|C_t)$ is

$$q(l_t|C_t) = \prod_{a\in A} q(l_t(a)|C_t(\omega)), \tag{14}$$

where $l_t(\omega)$ is the observation of the input data ω, consisting of the currently measured area in the images, such as data input intensity or gradients, and so on. From Eq. (7) to Eq. (14), spatial and temporal dependencies of the segments are unified by using a dynamic probabilistic model based on the conditional random field. In addition, the $S_a(C_{t+1}(\omega)|p_t(\rho))$ in (13) can measure the utility for observation sequences and create the discernibility matrix. Therefore, we can establish a utility matrix based on the above discernibility matrix(DM).

D. Restructure the discernibility matrix (DM) with Normalized Control Penalty(NCP) method

In Figure 2, after completing the sensitive object classification via privacy-preserving enhanced dynamic conditional random field (PPEDCRF) and filling in test data, we need to reconstruct the discernibility matrix (DM) according to the input data-set and classify the sensitive objects and create a relationship between sensitive (or privacy) classes and sensitive(or privacy) object region during the reconstruction stage. Therefore, the classification matrix (CM) can be formatted and

matched with the discernibility matrix; the DM [28] [29] can be measured by using the classification matrix(CM).

In this paper, we extend the increased edge penalty (IEP) [30] to estimate the sensitive visual objects and find similar regions. Thus, we introduce the normalized control penalty (NCP) method, which can measure the loss of information by using an acceptable accuracy rate. In the case of classification, the NCP method is defined as related to the hierarchy. Thus, the sensitive classes and non-sensitive classes can be defined as a tree architecture, and the relationship tree can associate all the input classification image tags according to the privacy score and type correlation carried in the CM, and adjust the tree according to the NCP to protect the privacy of sensitive and related categories. The deterministic punishment NCP mainly includes:

1) **The measure matrix for numerical attributes**: We consider Table T with classified label $(A_1, \ldots, A_n)$ from classification matrix. We assume that sequence images as tuple $r = (y_1, \ldots, y_n)$ will be a new node in the tree is generalized to tuple $r' = ([x_1, z_1], \ldots, [x_n, z_n])$ where x_n and z_n are two nodes from the tree, and the tuple r with their attribute A_i can be processed by NCP, r can be used as the hierarchical tree node in the hierarchical tree. The NCP equation is shown as follows.

$$NCP_{A_i}(r) = \frac{\{z_i\} - \{y_i\}}{\{x_i\} - \{y_i\}}, \tag{15}$$

where

$$|A_i| = \max_{r \in T} r.A_i - \min_{r \in T} r.A_i. \tag{16}$$

2) **The utility matrix of classified and sensitive attributes**: In the classification stage, the sensitive attributes can be generalized in batches to build a hierarchical tree according to the relationship of the sensitive attributes of the detected objects, which specifies attributes with different regularities. Therefore, after scanning and inputting the test image, we can perform tree traversal according to the similar attributes of the tested object. If the corresponding leaf node is accessed, we can correspond to the tested object in the original data according to the label associated with the leaf node. class location. We assume that many leaf nodes create a hierarchical tree v. For the categorical attribute A_i, v is generalized to their leaf nodes $\{v_1, \ldots, v_m\}$ to form the affiliation of sensitive attributes. Generally, the closer to the root node, the better the generalization of sensitive classes. good. We found that the features of ancestors can extract features from different target classes and determine the depth of the tree (v_1 is the root node and its left leaf is v_2), which is represented by the number of leaf nodes in the hierarchical tree.

$$NCP_{A_i}(r) = \frac{|Attribute(v_1, \ldots, v_m)|}{A_i}, \tag{17}$$

where $|A_i|$ is the number of A_i , and $Attribute(v_1, \ldots, v_i)$ are the set of values generalized by classification matrix CM, input in (14). We have

$$v_i = q(l_i|p_i) = \Pi_{NCP_{A_i}(r) \in A_i} q(l_t(NCP_{A_i}(r))|p_t(NCP_{A_i}(r))). \tag{18}$$

Intuitively,

1) For the confidential of object attribute A_i, $NCP_{A_i}(r)$ can measure how many images from r are generalized based on the attribute A_i which measures the generalized interval size;
2) For the classification attribute A_i, $NCP_{A_i}(r)$ measures how many images from r are generated on A_i in terms of the number covered by the generalized one.

Considering both confidential and classification attributes, we define the weighted normalization of the tuple r to determine the penalty.

$$NCP(r) = \sum_{i=1}^{n} (w_i \cdot NCP_{A_i}(r)), \sum_{i=1}^{n} w_i = 1. \tag{19}$$

In addition, the weighted normalized positive penalty of table T is defined as

$$NCP(T) = \sum_{r \in T} NCP(r). \tag{20}$$

In addition, we introduce a loss measurement to reflect the impact of the sensitive degree of DM, which is named a multilevel mining loss function (ML_2). This measurement represents the loss of visual data for visual object detection with frequent multilevel sets whilst matching the region of interest from the classified objects region instead of the original unclassified data set.

Mining classes and features at multiple privacy levels are to find the interests via using data mining and tree traversal from the created tree, since it allows the object detection with frequent association rules and frequent object sets that may not appear in the classes.

It can save an unnecessary process to use a generalization-based method to measure original data privacy, since the frequent features at the lower level of the hierarchical structure can be ignored. The correlation between the labelled classes can be detected at a higher level of privacy. ML_2 represents the proportion of all frequent data-sets that do not appear at the appropriate induction level if the multilevel tree is recognised instead of the original unclassified data-set. This is expressed as

$$ML_2(D) = 1 - \frac{\sum_i^h FI_i(v^p)}{\sum_i^h FI_i(v)}, \tag{21}$$

where FI_i returns the number of frequent data-sets of generalized level i, and the leaf node v^p and v can be calculated by (18) in sensitive classes and non-sensitive (non-privacy) data-sets, respectively.

We further strengthen the observation of information loss in multilevel trees via calculating the difference between the generalized levels of the frequent items that appear in the original data and its generalized level that appeared in classified data.

E. Feature-space Noise Injection and Reconstruction

Our goal is to protect location privacy against background-based matching attacks by perturbing *location-sensitive feature components* rather than model gradients. Given an input frame I_t, we extract its feature representation $z_t = f(I_t)$, where $f(\cdot)$ can be a hand-crafted descriptor (e.g., SIFT) or a learned embedding (e.g., CNN patch tokens). PPEDCRF first updates the discernibility matrix DM via temporal-spatial consistency and infers a sensitive mask M_t that selects background-related sensitive features/patches. The Normalized Control Penalty (NCP) then outputs a sensitivity score $\alpha_t \in [0, 1]$ which controls the perturbation magnitude.

We inject Gaussian noise only on the sensitive components:

$$\tilde{z}_t = z_t + M_t \odot \epsilon_t, \qquad \epsilon_t \sim \mathcal{N}(0, \sigma_t^2 I), \tag{22}$$

where $\odot$ denotes element-wise product and $\sigma_t = \sigma_0 \cdot \alpha_t$ is the frame-wise noise scale. Optionally, if the system needs to release sanitized videos rather than features, we reconstruct a sanitized frame I'_t by feature inversion:

$$I'_t = \arg\min_I \ \|f(I) - \tilde{z}_t\|_2^2 + \lambda \, \mathrm{TV}(I), \tag{23}$$

which preserves overall perceptual quality while suppressing location-sensitive signatures in the background.

$$\nabla_\lambda L_{SGA} = \sum_{n=1}^{N} \sum_{t=1}^{T} [f(b_{t+1}, b_t, a^{(i)}) - \sum_{b_{t-1}} \sum_{b_t} p(b_{t-1}, b_t \cdot f(b_{t-1}, b_t, a^{(i)}))] \tag{24}$$

In order to protect ε-deferential privacy of images via our proposed PPEDCRF, we output the tree node $r = y_1, y_2 \ldots y_n$ from existing the objects with their region features. The method is tuned for the parameters, which means the learning process is still divergent compared with the original stochastic gradient descent (SGD) method. The SGD and SGA can convert from each other according to the optimization method [31].

F. Noise generating

After finding the privacy protection solution in CRF relying on PPSGA, we confirm that the whole process for our proposed solution PPEDCRF, which deals with the images with four steps as shown in Figure 2.

At first, we use the classes for classification matrix as $v_1, v_2, \ldots v_N$. We import the parameters of loss function, learning rate, and noise scales with the adjacent matrix x.

Next, we establish the discernibility matrix according to the training set Θ and classes. Following PPEDCRF, the DM will be updated via using the adjacent matrix x.

After collecting the samples in the third step, in the forth step, the algorithm will restructure the DM corresponding to the samples in $\mathcal{X}$, where we set object detection model as $Det(M)$. In our proposed algorithm, we use YOLOv4 [32] as the object detection model. After the object detection is completed, the framework will return the result containing the matched results. Then, we add calibrated Gaussian noise into the inferred sensitive segments of the test images (clipped Gaussian mechanism).

Algorithm 1 PPEDCRF with Feature-space Noise Injection

Input: image sequence $\mathcal{X} = \{I_t\}_{t=1}^T$, sensitive classes $\{D_n\}_{n=1}^N$, adjacency matrix x, feature extractor $f(\cdot)$ (e.g., SIFT/CNN embedding), optional reconstructor $g(\cdot)$, dynamic-CRF parameters Φ, NCP parameters Γ, base noise multiplier σ_0.

Output: sanitized sequence $\mathcal{X}' = \{I'_t\}_{t=1}^T$ (or sanitized features $\tilde{\mathcal{Z}} = \{\tilde{z}_t\}_{t=1}^T$), sensitive masks $M = \{M_t\}_{t=1}^T$, and privacy cost (ρ, ω).

procedure PPEDCRF_FUTURENOISE($\mathcal{X}$)
  $\{D_n\}$, x, f, g, Φ, Γ, σ_0
  $DM \leftarrow \mathbf{0}$
  for $t \leftarrow 1$ to T **do**
    $z_t \leftarrow f(I_t)$
    $l_t \leftarrow \mathrm{Obs}(z_t)$ ▷ e.g., keypoints/descriptors or patch embeddings
    $DM \leftarrow \mathrm{DCRFUpdate}(DM, l_t, x; \Phi)$
    $M_t \leftarrow \mathrm{Mask}(DM, \{D_n\})$ ▷ sensitive features/patches
    $\alpha_t \leftarrow \mathrm{NCP}(DM, M_t; \Gamma)$
    $\sigma_t \leftarrow \sigma_0 \cdot \alpha_t$
    $\epsilon_t \sim \mathcal{N}(0, \sigma_t^2 I)$
    $\tilde{z}_t \leftarrow z_t + (M_t \odot \epsilon_t)$
  Option A (publish features): store $\tilde{z}_t$
  Option B (publish images): $I'_t \leftarrow g(\tilde{z}_t, I_t)$ ▷ feature inversion / decoder
  end for
  $(\rho, \omega) \leftarrow \mathrm{PrivacyCost}(M, \{\alpha_t\}_{t=1}^T)$
  return $\mathcal{X}'$ (or $\tilde{\mathcal{Z}}$), M, (ρ, ω)
end procedure

During the training, the model parameters are utilized to minimize the empirical deficit function $L(\Theta)$. The parameters are applied to control the whole process of convergence, as the PPEDCRF parameters are able to be obtained and optimized through the model training. Thus the whole process of Privacy-preserving Enhanced Dynamic Conditional Random Field(PPEDCRF) Algorithm can be created.

G. Privacy-preserving Enhanced Dynamic Conditional Random Field(PPEDCRF) Algorithm

After describes the whole process, we can expand the algorithm. In Algorithm 1, the raw input image data-sets Θ and the labeled data-sets with all objects belong to sensitive classes $D_1, D_2, \ldots D_N$. The size of the class N means the number of classes. The adjacent matrix x is the feature matrix saving the features from Θ and the loss function is the proposed loss function, and the noise scale τ is the range of noise sub-sampling, and the gradient norm bound G is the bound in SGD iteration. The output is the processed dataset Θ' and privacy cost (ρ, ω). In the process stage, each training iteration will generate the parameters $P_n(\eta, \tau, G)$ from Dynamic Conditional Random Filed method, which will help calculate the privacy score S from Θ and in each SGD stage.

In each frame, PPEDCRF injects calibrated Gaussian noise

TABLE I: Datasets and their roles in evaluation.

Dataset	Usage in this paper
MOT16 / MOT17	Detection/segmentation utility evaluation (mAP, recall/-precision) on driving-like sequences.
Cityscapes	Additional segmentation utility evaluation on urban scenes.
KITTI	Additional detection utility evaluation on driving scenes.
VOC2008	detector-only sanity check.
Street-view database	Location-privacy attack evaluation (Top-k retrieval / Recall@k).

into *location-sensitive feature components* selected by the mask M_t, rather than perturbing model gradients.

In our implementation, noise is injected in the feature space to directly disrupt location-retrieval cues. If the system releases sanitized videos, we reconstruct I'_t by solving a feature-inversion problem: $\min_{I'_t} \|f(I'_t) - \tilde{z}_t\|_2^2 + \lambda \mathrm{TV}(I'_t)$, so that the released frame preserves overall visual utility while removing location-sensitive background signatures.

III. Experimental Evaluations

We evaluate the performance of the proposed method based on a machine equipped with central processing unit (CPU) Intel Core (TM) i7 @2.4 GigaHertz (GHz), Microsoft Windows 10 (64 bits) operating system, and GeForce RTX 3070 Graphics Card with 8 Gigabytes (GB) memory and Compute Unified Device Architecture (CUDA) version 11.0. The data labels and test images have been obtained from MOT Challenge 2016 data-set [19].

A. The performance of PPEDCRF and NCP for object detection

In order to evaluate how PPEDCRF affects object detection performance, we conduct the main driving-sequence experiments on MOT16/17, Cityscapes, and KITTI as summarized in Table I. We additionally report a detector-only sanity check on VOC2008 [33].

- In Figure 3, we list the experimental results with and without PPEDCRF+NCP, the experiments show the results are the curves for "Faster RCNN and Privacy-preserving deep learning" based on the solution via Faster R-CNN [6] and privacy-preserving [6] to detect the visual objects and using federated learning [8] for privacy preservation. The other curve named "YOLO+baseline privacy methods"(without PPEDCRF+NCP) shows the experimental results based on YOLO-DarkNet [32] for object detection and federated learning [34] for privacy protection. Those two curves don't use without PPED-CRF+NCP.
- **GIoU loss** in Fig. 3 (lower is better) in Figure 3 is based on Faster RCNN + Federated learning (FRFL), YOLOV4 + federated learning (YFL), YOLOV4 + federated learning + PPEDCRF (YFLP), and YOLOV4 + federated learning + PPEDCRF+ NCP (YFLPN) whose GIoU values are in 200 epochs. Overall, the GIoU values of FRFL, YFL, YFLP, and YFLPN all decrease with the number of epochs. The GIoU values of the four models drop rapidly in the first hundred epochs and tend to regress thereafter. After 200 epochs, the FRFL drops from about 0.9 to 0.3. YFL and YFLP roughly coincide, dropping from about 0.7 to 0.2, while YFLPN drops from about 0.4 to 0.1. Therefore, under the GIoU loss metric, a smaller value indicates better box regression quality, and YFLPN achieves the lowest loss among the compared methods.
- The "Objectness" rates in Figure 3 have 200 epochs. It is clear that the Classification values of FRFL, YFL, YFLP, and YFLPN all decrease with the number of epochs, but YFLPN reaches a global minimum of about 0.015 at 200 epochs, after which it is predicted to rise. Both FRFL and YFLP begin to decrease from about 0.07, with the former falling to 0.03 and the latter falling by up to about 0.05 to 0.02. YFL and YFLPN drop from 0.04 to around 0.2. In this sub-figure, it can be seen from the figure that the best detection effect at 200 epochs is the YFLPN method, followed by YFL, followed by YFLP, and FRFL has the worst performance effect.
- The "classification" rates in Figure 3 also have 200 epochs, which shows that the precision value of all four methods increases with the number of epochs. YFLP and YFLPN grow the fastest, reaching a maximum of nearly 0.9 around 150 times and decreasing to about 0.8 as the number of epochs increased.YFL as a whole is regression, predicting nearly 0.8 in 250 epochs. On the other hand, FRFL rises slowly over 100 to 200 epochs, rises slightly faster after 0 to 100 and 200 epochs, and finally rises to about 0.6. Therefore, from the images, it can be seen that YFLP and YFLPN have the highest recognition accuracy, followed by YFL and rise steadily, and FRFL has the lowest accuracy.
- The "Precision rate mAP@0.5" in Figure 3 also shows those four methods increase with the number of 200 epochs. YFLP and YFLPN grow the fastest, reaching a maximum of nearly 0.9 around 150 times and decreasing to about 0.8 as the number of epochs increased.YFL as a whole is regression, predicting nearly 0.8 in 250 epochs. On the other hand, FRFL rises slowly over 100 to 200 epochs, rises slightly faster after 0 to 100 and 200 epochs, and finally rises to about 0.6. For this sub-figure, it can be seen that YFLP and YFLPN have the highest recognition accuracy, followed by YFL and rise steadily, and FRFL has the lowest accuracy.
- The last sub-figure named "Recall rate mAP@0.5" in Figure 3 presents the "Recall" rates of those four methods increase with the number of epochs. FRFL and YFL rise slightly more slowly, with an approximate regression, reaching 0.6 after 200 epochs and 0.9 after 300 predictions.YFLPN rises faster, reaching a maximum of about 0.95 at about 200 epochs, and then decreases to about 0.9 with the increase in the number of epochs. The YFLP rise is similar to YFLPN, reaching a maximum of about 0.9 in 150 epochs, and then predicts that it will decrease first as the number of epochs increases, and then increases as the number of epochs increases, reaching 0.9 after 300 epochs. Therefore, at 200 epochs, YFLP has the highest accuracy, followed by YFLPN, and YFL and FRFL have

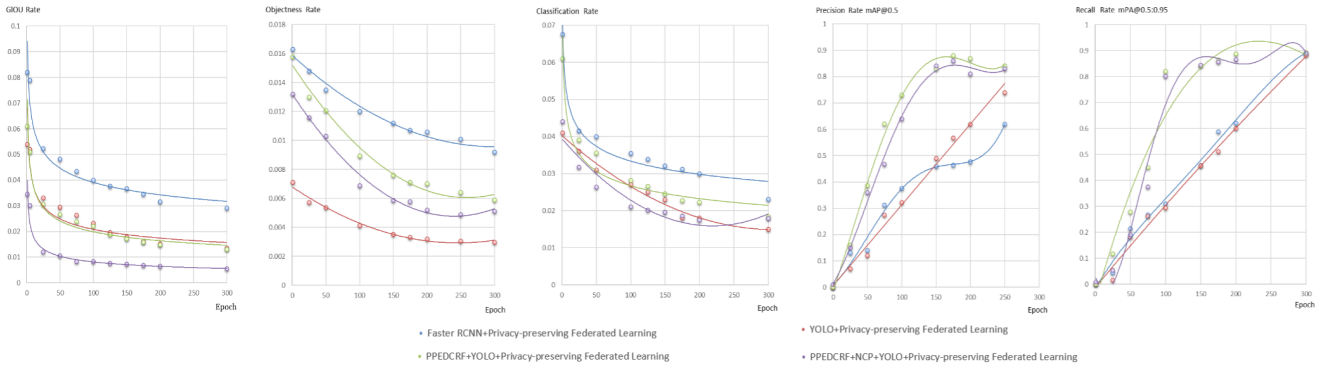

Fig. 3: The performance of objects detection with and without PPEDCRF+NCP

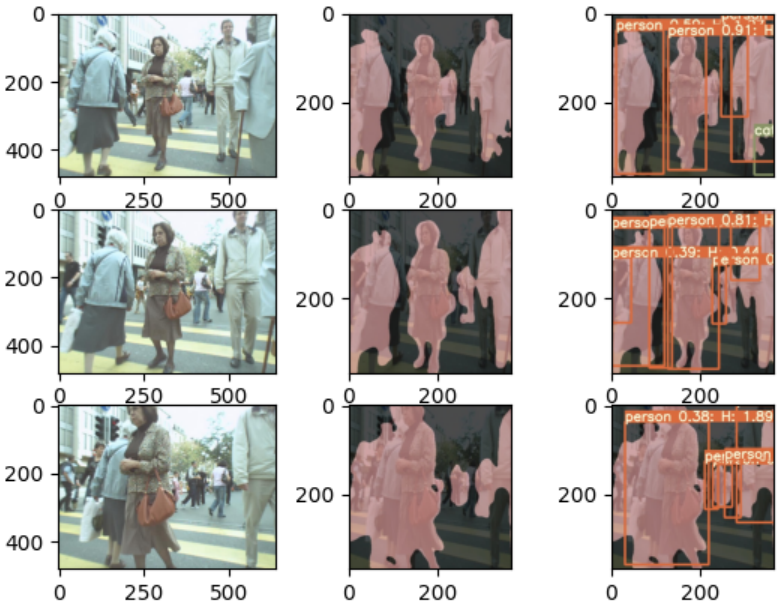

Fig. 4: Predict Result on Privacy-preserving Enhanced Dynamic Conditional Random Field (PPEDCRF)

the lowest accuracy.

- From those five indexes, YFL performed consistently on all five indicators, especially objectness, which was significantly better than several other methods. Although the effect of YFLPN proposed in this paper is affected by privacy protection to a certain extent, its performance is not much worse than that of YFL without adding a privacy protection mechanism and even performs better in GIoU and precision. However, compared to YFLP, which has added other privacy protection methods, its indicators are better in all aspects. FRFL had the worst effect on all five indicators in the experiment.

The experimental results are presented in Figure 3. As shown in Figure 3, the performance of object detection is efficient with Faster R-CNN and YOLOv4, since the object detection is before autopilot, and we mainly test the solutions of object detection for various privacy protection.

In this experiment, the AP (Average Precision) values are calculated by $AP = \frac{1}{11}\sum_{r\in\{0,0.1,\ldots,1\}} P_{intercept}(r)$, which refers to the calculation method in VOC2008 challenge [33] for detector-only sanity check. The mean Average Precision(mAP) values are calculated via computing again the average value over the classes number, $mAP = \frac{\sum_{q=1}^{Q} AP(q)}{Q}$, and Q denotes the classes number.

Firstly, we begin the test with the threshold of mean average precision (mAP) as 0.5 ($mAP_{0.5}$), which means that the prediction is positive if $IoU \geq 0.5$. In Figure 3, the curve of mAP increases constantly, the range of mAP is within 0.5 which corresponds to the general range of an effective object detector. For mAP, the convergence is not presented in Figure 3 but the increasing trend still remains during the over 200 epochs. The reason is that our proposed two-stage structure

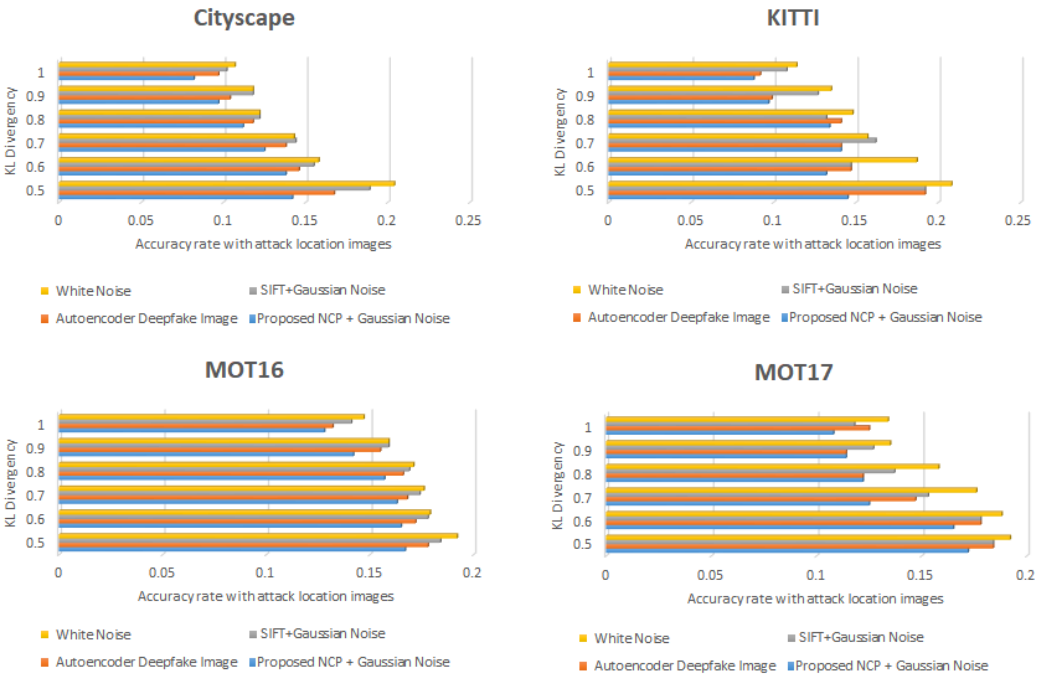

Fig. 5: Comparison of privacy-preserving performance for detection task

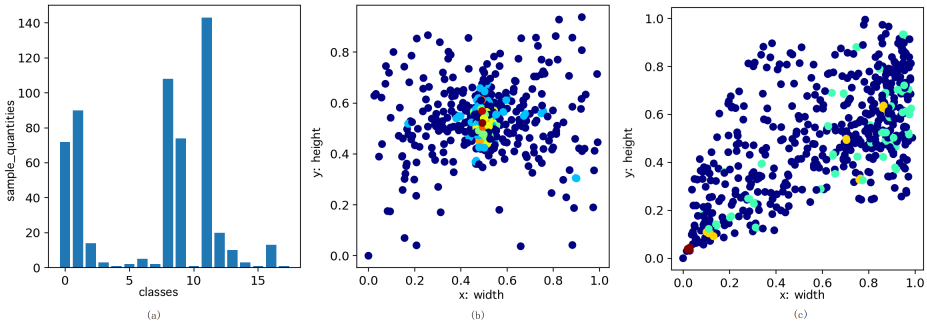

Fig. 6: Performance of classification with YOLOV4 under the PPEDCRF

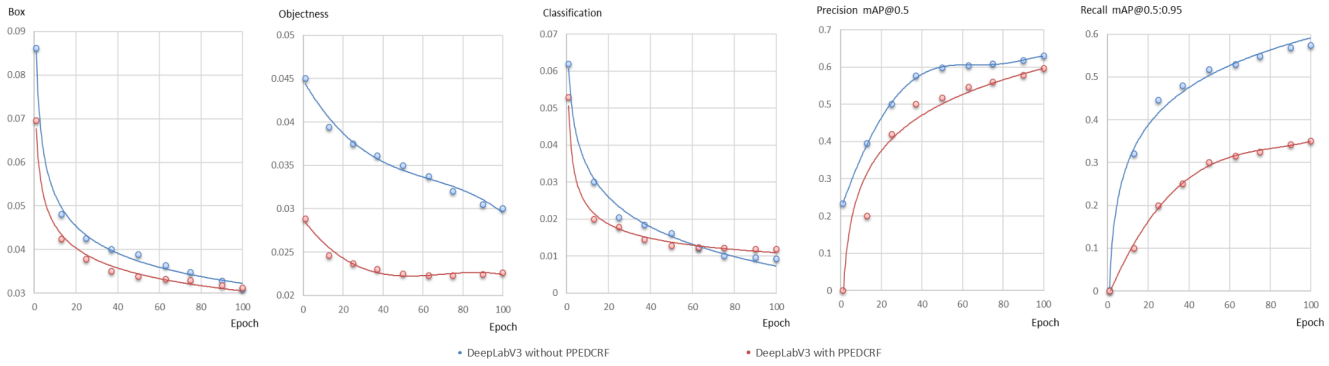

Fig. 7: The performance of Segmentation for DeeplabV3 without PPEDCRF(1st Row) and with PPEDCRF(2nd Row)

and more epochs are required to get the same accuracy of the classifications. Besides, we also set multiple IoU thresholds from 0.5 to 0.95 with a step size of 0.05. The mAP 0.5:0.95 values are increasing during over 200 epochs and the overall mAP increases from 0 to 0.92 if the proposed PPEDCRF is applied inside of the detector, while the overall mAP in the

other privacy-preserving method [8] only increases from 0 to 0.77.

Although the curve of **GIoU loss** decreases over training, the final loss approaches 0.005, indicating improved box regression quality under the adopted definition (lower is better). Compared with the detector based on our PPEDCRF solution, there are no significant differences between [6] and the PPEDCRF solution. For the classification scores [35], we conclude that the PPEDCRF has fewer negative effects on the prediction results because PPEDCRF separately copes with both sensitive areas and sensitive classes, and the YOLO [32] with preserving-preserving methods approach the same as well. The inference results for PPEDCRF is shown in Figure 4.

B. The Utility analysis of Normalized Control Penalty(NCP) in PPEDCRF

In order to further demonstrate the validity of the privacy of the proposed solution, in Figure 5, the tests have been conducted based on real-world benchmarks, which used Cityscapes [36], KITTI [37], MOT16 and MOT17 [19], four data sets related to object detection with series pictures.

MOT17 is mainly aimed at moving pedestrians and vehicles, compared to MOT16 with detailed annotations, and more bounding box datasets, MOT17 has richer image content, and it also contains different weather conditions video. There are actually twelve categories in the MOT16 and MOT17 data set, and we chose eight classes(three of them are sensitive classes). From the features of the test images, we see that MOT16 consists of eight categories and has an uneven distribution, and MOT16 mainly marks moving objects. Besides, MOT17 also has three sensitive relative classes, they are pedestrian, person on vehicle, and static person, whole three classes contain approximately 280 samples. Similar to MOT16, MOT17 mainly contains street view images around 50 different cities, including 5000 high-quality pixel-level annotated images of driving scenes in urban environments (MOT17 increased to 2975 samples in train class, 500 in validation class, and 1525 in tests classes, 19 categories); In addition, there are 20,000 coarse labeled images. And The KITTI dataset uses assembled well-equipped acquisition vehicles to collect data on actual traffic scenarios.

PPEDCRF adds sampling noise to sensitive classes to prevent feature extraction attacks. For the defense test of this type of attack, it is necessary to sample the data of the tracking object area and compare different noise addition methods to test whether the data feature distribution under privacy protection is the same and similar to the data distribution feature before processing. The KL divergence method measures the distribution similarity of samples. This test is generated by extracting a sensitive subset (pedestrian category) from the original data set. The X-axis represents the attack accuracy from privacy protection under a specific KL divergence. The attack accuracy is the accuracy rate at which the attacker can match the target object from the sensitive features. And the Y-axis represents the KL divergence value relative to the original data set. In Figure 5, the proposed method in this paper is denoted as Proposed NCP+Gaussian Noise, and the other three comparative privacy protection methods are Autoencoder Deepfake Image (ADI) [38], SIFT+Gaussian Noise (SGN) [39], and the work with directly adding White Noises (WN) [40].

In Figure 5, we use different colors to distinguish the four methods. And the figure shows the accuracy of the attacker under the same KL divergence (same privacy level) level that the four methods are subjected to privacy attacks. The KL divergence ranges from 0.5 to 1, and the step size is 0.1, which represents the original target data and the corresponding method to add noise data. The relative entropy between the subsequent data. As we can see, when the KL divergence is 0.5, all attacks can achieve the highest accuracy in obtaining privacy. This shows that the sampling rate and prevention effect of the protection method increase with the increase of the KL divergence because the KL divergence increases. Except that the accuracy of the white noise (WN) method of the KITTI dataset is slightly higher than 0.2, the maximum accuracy of the four privacy protection methods is less than 0.2 for the attacker when the KL divergence on the four different datasets is higher than 0.5. In the Cityscape data set, our method achieves the lowest accuracy rate than the other three methods such as ADI and SGN when the KL divergence is 0.5, and is lower than the other three methods under different divergence conditions, so this article Overall it is more effective. If the four algorithms are applied to the MOT16 and MOT17 data sets, the same performance will also be presented. The performance of SGN drops slightly when using the KITTI and MOT16 datasets (high attack accuracy). For example, the KL divergence is 0.8 and 1, respectively, but compared with the Autoencoder Deepfake Image (ADI) method, the SGN method gains a high accuracy of privacy. On the same KL divergence, white noise (WN) always has a higher attack accuracy than the other three methods, indicating that its privacy protection ability is the weakest.

Finally, Figure 5 shows the reasoning results of PPEDCRF in YOLO, where the test data set and results from the sequence frames in the video clip show that all moving objects have been segmented and detected, and the results of the background image have been protected. The results show that, with our proposed privacy-preserving method, it is difficult for an attacker to find the background locations of sensitive classes on the object dataset. Therefore, we believe that the proposed method in this paper has protected the privacy of the object's location in tasks such as object recognition and segmentation.

Figure 6 clearly shows the effectiveness of our proposed algorithm (NCP). The horizontal and vertical axes represent the samples in 2-dimensional (2D) space, respectively. As shown in Figure 6, the distribution of the samples is close and the features cannot be accurately extracted by using the detector, and the NCP effectively reduces the data points in the center of the map. A more decentralized global structure is also revealed. A similar advantage is also shown in the tests based on the KITTI data set. A more uneven data distribution is involved in the KITTI data set, but the distance between data points is presented according to the visualization result. We use different colors to distinguish these features. In addition, according to the complexity analysis of NCP, its running time

is controlled by the function $|t_c|$. Therefore, given $|t_c|$, we propose that the running time of NCP is shown in Figure 5. The test set is generated by randomly extracting subsets from the original data set.

Since this test involves KL Divergence, Figure 6 clearly shows the classification of categories and sample distributions under our combined detection (PPEDCRF+YOLOV4) for object detection. This test uses the MOT16 [19] data set. Figure 6(a) is the sample size of each type distribution, the x-axis is the class number and the y-axis is the number of samples in the corresponding class. It can be seen that the class distribution is unbalanced. Some classes have a small number of samples, while some classes have a large number of samples. Figure 6(b) and (c) are sample distributions, and the x and y axes are length units, representing the samples before (b) and after NCP processing (c) on the relationship tree. The sample similarity distance, the more similar the closer the sample distance. And the non-private sample features are marked in blue and the privacy features are marked in other colors (the redder indicates the higher the privacy level of the sample). It can be seen that the privacy class is very close before NCP processing, so after the attacker matches one type of privacy class, the easier it is to match other similar privacy classes. After NCP processing, the distribution of all samples has changed. And the distance between privacy classes becomes larger, and it becomes more and more difficult for attackers to match other privacy classes by imitating the cracked privacy class.

C. Performance of object detection with privacy-preserving and non privacy protection

Several measures were leveraged to evaluate the detector's performance with or without PPEDCRF, and this test will evaluate the performance of the proposed method on the segmentation task. Figure 7 illustrates the implementation of object segmentation without PPEDCRF in the first method and with PPEDCRF in the second method by using DeepLabV3 [41].

- The sub-figure of the "Box" rate in Figure 7 describes the detection box rates of DeepLabV3+ PPEDCRF(short name as DL+P) and DeepLabV3(short name as DL) over 100 epochs. In general, both the box rates of DL+P and DL decrease with the number of epochs. The curves of the two models basically coincide, and the decrease rate is faster in the first 200 epochs, and the decrease rate is slower after that, and they tend to regress. After 100 epochs, DL drops from around 0.09 to 0.03, while DL+P drops from 0.07 to 0.03. So from the graph, the two models perform similarly on the "Box" indicator.
- The sub-figure of "Objectness" rate in Figure 7 describes the detection objectness rates of DeepLabV3+ PPEDCRF(short name as DL+P) and DeepLabV3(short name as DL) over 100 epochs. Overall, both the objectness rates for DL+P and DL decrease with the number of epochs. However, the two models differ significantly in objectness rates, with DL dropping from 0.045 to 0.03, falling slightly faster before 50 epochs than after 50 epochs. While DL+P drops from around 0.03 to 0.021, its first 40 epochs decrease slightly faster, and the subsequent decrease rate very slowly. So from the graph, the DL+P model performs better than DL on the objectness indicator.
- The figure of "Classification" rate in Figure 7 describes the detection classification rates of DeepLabV3+ PPEDCRF(short name as DL+P) and DeepLabV3(short name as DL) over 100 epochs. In general, both the classification rates of DL+P and DL decrease as the number of epochs increases. The curves of the two models basically coincide, and the decrease rate is faster in the first forty epochs, and the decrease rate is significantly weakened and tends to regress after forty epochs. After 100 epochs, DL+P drops from around 0.05 to 0.01 and DL from around 0.06 to 0.01. So from the graph, the two models perform similar effects on the classification indicator.
- The figure of "Precision" rate in Figure 7 describes the detection precision rates of DeepLabV3+ PPEDCRF(short name as DL+P) and DeepLabV3(short name as DL) over 100 epochs. Overall, the precision rates of both DL+P and DL increase with the number of epochs. DL+P increases from 0 to around 0.6, and DL increases from about 0.2 to around 0.6, but the precision rate of DL is significantly higher than DL+P in a hundred iterations. The curves of both models grow faster in the first 40 epochs, DP grows slower after that, and DL grows very slowly after that. So from the graph, DL performs better than DL+P on the precision indicator.
- The figure of "Recall" rate in Figure 7 describes the detection recall rates of DeepLabV3+ PPEDCRF(short name as DL+P) and DeepLabV3(short name as DL) over 100 epochs. Overall, the recall rates for both DL+P and DL grow logarithmically, increasing with the number of epochs. During 100 epochs, however, DL grows significantly faster than DL+P increasing from 0 to 0.6, and DP increases from 0 to around 0.3. So from the graph, DL performs significantly better than DL+P on the recall indicator.
- From the experimental data, the PPEDCRF privacy protection method proposed in this paper combined with DeepLabV3 has a negative impact on the recall and precision indicators, but the impact is limited to around 0.2, and the effect on the objectness indicator is better than that of DeepLabV3 without the PPEDCRF method. The impact on the other two indicators is similar.

The curve of Box and Objectness fluctuates constantly. It has an extensive fluctuation range either in the "Recall" or in the "Precision" process, representing the training time that will impact the object segmentation. Figure 7 shows apparent trends in training and validation processes. Classification is a critical stage for segmentation. Regarding classification, the increased trend occurs during model training with both non-PPEDCRF and PPEDCRF. Besides, the recall increases while the predicted precision change to stable status. Pertaining to the mAP matrix, similar fluctuated trends are shown with multiple IoU (mAP@0.5, mAP@[.50:.05:.95]), and the final mAP is stable around 0.62(non-PPEDCRF) and 0.58(PPEDCRF),

respectively.

Due to the two-stage detector, the epochs are doubled compared with the experiments conducted with DeepLabV3. In Figure 7, though the curve of "IoU" remains the downward trend as before, the whole "Box" decreases from 0.08 $\sim$ 0.07 to 0.03 $\sim$ 0.02 during the training process. The same direction is presented in the objectness, approximately from 0.045 $\sim$ 0.028 to 0.03 $\sim$ 0.022. The test result shows the gap between the first and second rows in "Objectness," "Recall," and "Precision" is more significant than those in "Box" and "Classification." For those three more oversized gap items, the gap can be limited to less than 0.01, and "Precision" less than 0.2. This test can show some shortcomings of PPEDCRF, which may be overcome in our future works.

Compared with the detection results using only the DeepLab detector (without using any privacy-preserving method), the PPEDCRF classification curve gradually shows a convergence trend, while the overall convergence slows down. This classification experiment can show that PPEDCRF does not impair sample classification compared with the method without privacy protection. Notably, the precision stays high as its recall increases, demonstrating that our merged (PPEDCRF+DeepLab) detector has desirable performance.

IV. Conclusion

We have proposed an effective algorithm for protecting the privacy of the image background by using a conditional random field (CRF). Our proposed method is to find the balance between object detection and privacy protection. Our proposed solution is very different from those existing solutions with only simply adding noises in the whole image. In our evaluations, we have compared our proposed method with the existing privacy-preserving solutions [34] [42]. On one hand, the training convergence was faster than our proposed methods. On another hand, our proposed solution has high accuracy for autopilot object detection, since our proposed method deals with the sensitive areas in test images separately and brings fewer damages in object detection than other methods [34] [42]. By comparing different solutions through using the images with sensitive backgrounds from the datasets [18], we have shown that our proposed solutions have better performances in accuracy and speed. The performance of our proposed method is acceptable if combined with the framework YOLOv4 [20] [32]. Our solution has been applied to effectively protect the privacy of images against location matching. In the future, we would like to improve the speed of noise generation and privacy protection via using one stage framework for privacy preservation.

References

[1] M. Chamikara, P. Bertok, I. Khalil, D. Liu, and S. Camtepe, "Privacy preserving face recognition utilizing differential privacy," *Computers and Security*, vol. 97, p. 101951, 2020.

[2] Y. Li, Y. Wang, and D. Li, "Privacy-preserving lightweight face recognition," *Neurocomputing*, vol. 363, pp. 212–222, 2019.

[3] S. A. Ahmed, D. P. Dogra, S. Kar, and P. P. Roy, "Trajectory-based surveillance analysis: A survey," *IEEE Transactions on Circuits and Systems for Video Technology*, vol. 29, no. 7, pp. 1985–1997, 2018.

[4] P. Speciale, J. L. Schonberger, S. B. Kang, S. N. Sinha, and M. Pollefeys, "Privacy preserving image-based localization," in *Proceedings of the IEEE Conference on Computer Vision and Pattern Recognition*, 2019, pp. 5493–5503.

[5] L. Jiao, F. Zhang, F. Liu, S. Yang, L. Li, Z. Feng, and R. Qu, "A survey of deep learning-based object detection," *IEEE access*, vol. 7, pp. 128 837–128 868, 2019.

[6] S. Ren, K. He, R. Girshick, and J. Sun, "Faster R-CNN: Towards real-time object detection with region proposal networks," in *Advances in Neural Information Processing Systems*, 2015, pp. 91–99.

[7] Z. Ren, Y. J. Lee, and M. S. Ryoo, "Learning to anonymize faces for privacy preserving action detection," in *European Conference on Computer Vision*, 2018, pp. 620–636.

[8] Y. Liu, Z. Ma, X. Liu, S. Ma, and K. Ren, "Privacy-preserving object detection for medical images with faster r-cnn," *IEEE Transactions on Information Forensics and Security*, 2019.

[9] J. Zhou and C.-M. Pun, "Personal privacy protection via irrelevant faces tracking and pixelation in video live streaming," *IEEE Transactions on Information Forensics and Security*, vol. 16, pp. 1088–1103, 2020.

[10] Z. Zhang, P. Luo, C. C. Loy, and X. Tang, "Joint face representation adaptation and clustering in videos," in *European Conference on Computer Vision*. Springer, 2016, pp. 236–251.

[11] X. Wang, Z. Chen, J. Tang, B. Luo, Y. Wang, Y. Tian, and F. Wu, "Dynamic attention guided multi-trajectory analysis for single object tracking," *IEEE Transactions on Circuits and Systems for Video Technology*, vol. 31, no. 12, pp. 4895–4908, 2021.

[12] P. C. Roy and V. N. Boddeti, "Mitigating information leakage in image representations: A maximum entropy approach," in *Proceedings of the IEEE Conference on Computer Vision and Pattern Recognition*, 2019, pp. 2586–2594.

[13] Y. Dodis and A. Smith, "Correcting errors without leaking partial information," in *Proceedings of the thirty-seventh annual ACM symposium on Theory of computing*, 2005, pp. 654–663.

[14] H. Wang, S. Xie, and Y. Hong, "Videodp: A flexible platform for video analytics with differential privacy," *Proceedings on Privacy Enhancing Technologies*, vol. 2020, no. 4, pp. 277–296, 2020.

[15] B. Balle and Y.-X. Wang, "Improving the gaussian mechanism for differential privacy: Analytical calibration and optimal denoising," *arXiv preprint arXiv:1805.06530*, 2018.

[16] Y. Wang, K.-F. Loe, and J.-K. Wu, "A dynamic conditional random field model for foreground and shadow segmentation," *IEEE Transactions on Pattern Analysis And Machine Intelligence*, vol. 28, no. 2, pp. 279–289, 2005.

[17] A. Shimada, D. Arita, and R.-i. Taniguchi, "Dynamic control of adaptive mixture-of-gaussians background model," in *IEEE International Conference on Video and Signal Based Surveillance*. IEEE, 2006, pp. 5–5.

[18] L. Lealtaixé, A. Milan, I. Reid, S. Roth, and K. Schindler, "MOT challenge 2015: Towards a benchmark for multi-target tracking," *arXiv preprint arXiv:1504.01942*, 2015.

[19] A. Milan, L. Leal-Taixé, I. Reid, S. Roth, and K. Schindler, "MOT16: A benchmark for multi-object tracking," *arXiv preprint arXiv:1603.00831*, 2016.

[20] J. Redmon, S. Divvala, R. Girshick, and A. Farhadi, "You only look once: Unified, real-time object detection," in *IEEE Conference on Computer Vision and Pattern Recognition*, 2016, pp. 779–788.

[21] W. Cheung and G. Hamarneh, "n-SIFT: n-dimensional scale invariant feature transform," *IEEE Transactions on Image Processing*, vol. 18, no. 9, pp. 2012–2021, 2009.

[22] Z. Wang, A. C. Bovik, H. R. Sheikh, and E. P. Simoncelli, "Image quality assessment: from error visibility to structural similarity," *IEEE Transactions On Image Processing*, vol. 13, no. 4, pp. 600–612, 2004.

[23] H.-J. Xing and X.-Z. Wang, "Selective ensemble of SVDDs with Rényi entropy based diversity measure," *Pattern Recognition*, vol. 61, pp. 185–196, 2017.

[24] M. Glodek, S. Scherer, and F. Schwenker, "Conditioned hidden markov model fusion for multimodal classification," in *Twelfth Annual Conference of the International Speech Communication Association*, 2011.

[25] J. Diebel and S. Thrun, "An application of markov random fields to range sensing," *Advances in neural information processing systems*, vol. 18, 2005.

[26] N. Chandgotia, "Generalisation of the hammersley-clifford theorem on bipartite graphs," *Transactions of the American Mathematical Society*, vol. 369, no. 10, pp. 7107–7137, 2017.

[27] B. Koo, M. Yoon, and S. Cho, "Isogeometric shape design sensitivity analysis using transformed basis functions for Kronecker delta property," *Computer Methods in Applied Mechanics and Engineering*, vol. 253, pp. 505–516, 2013.

[28] Y. Yao and Y. Zhao, "Discernibility matrix simplification for constructing attribute reducts," *Information Sciences*, vol. 179, no. 7, pp. 867–882, 2009.

[29] H.-y. Zhou and T. Yang, "A more efficient algorithm for attribute reduction based on the binary discernible matrix," *Computer Engineering and Design*, vol. 12, 2003.

[30] A. K. Qin and D. A. Clausi, "Multivariate image segmentation using semantic region growing with adaptive edge penalty," *IEEE Transactions on Image Processing*, vol. 19, no. 8, pp. 2157–2170, 2010.

[31] N. Loizou, H. Berard, G. Gidel, I. Mitliagkas, and S. Lacoste-Julien, "Stochastic gradient descent-ascent and consensus optimization for smooth games: Convergence analysis under expected co-coercivity," *Advances in Neural Information Processing Systems*, vol. 34, 2021.

[32] A. Bochkovskiy, C.-Y. Wang, and H.-Y. M. Liao, "YOLOv4: Optimal speed and accuracy of object detection," *arXiv preprint arXiv:2004.10934*, 2020.

[33] D. Hoiem, S. K. Divvala, and J. H. Hays, "Pascal VOC 2008 challenge," in *PASCAL Challenge Workshop in ECCV*. Citeseer, 2009.

[34] G. A. Kaissis, M. R. Makowski, D. Rückert, and R. F. Braren, "Secure, privacy-preserving and federated machine learning in medical imaging," *Nature Machine Intelligence*, pp. 1–7, 2020.

[35] M.-M. Cheng, Z. Zhang, W.-Y. Lin, and P. Torr, "BING: Binarized normed gradients for objectness estimation at 300fps," in *IEEE Conference on Computer Vision and Pattern Recognition*, 2014, pp. 3286–3293.

[36] M. Cordts, M. Omran, S. Ramos, T. Rehfeld, M. Enzweiler, R. Benenson, U. Franke, S. Roth, and B. Schiele, "The cityscapes dataset for semantic urban scene understanding," in *IEEE Conference on Computer Vision and Pattern Recognition*, 2016, pp. 3213–3223.

[37] A. Geiger, P. Lenz, C. Stiller, and R. Urtasun, "Vision meets robotics: The kitti dataset," *The International Journal of Robotics Research*, vol. 32, no. 11, pp. 1231–1237, 2013.

[38] H. Khalid and S. S. Woo, "OC-FakeDect: Classifying deepfakes using one-class variational autoencoder," in *Proceedings of the IEEE/CVF Conference on Computer Vision and Pattern Recognition Workshops*, 2020, pp. 656–657.

[39] E. Rublee, V. Rabaud, K. Konolige, and G. Bradski, "ORB: An efficient alternative to SIFT or SURF," in *International Conference on Computer Vision*. Ieee, 2011, pp. 2564–2571.

[40] H.-H. Kuo, *White Noise Distribution Theory*. CRC press, 2018.

[41] L.-C. Chen, G. Papandreou, I. Kokkinos, K. Murphy, and A. L. Yuille, "Deeplab: Semantic image segmentation with deep convolutional nets, atrous convolution, and fully connected CRFs," *IEEE Transactions on Pattern Analysis and Machine Intelligence*, vol. 40, no. 4, pp. 834–848, 2017.

[42] W. Li, F. Milletarì, D. Xu, N. Rieke, J. Hancox, W. Zhu, M. Baust, Y. Cheng, S. Ourselin, M. J. Cardoso *et al.*, "Privacy-preserving federated brain tumour segmentation," in *International Workshop on Machine Learning in Medical Imaging*. Springer, 2019, pp. 133–141.